InAs quantum dots: Predicted electronic structure of free-standing versus GaAs-embedded structures

A. J. Williamson and Alex Zunger
National Renewable Energy Laboratory, Golden, Colorado 80401
~Received 22 October 1998!

Using an atomistic pseudopotential approach, we have contrasted the ~i! strain profiles, ~ii! strain-modified band offsets, ~iii! energies of confined electrons and holes, and ~iv! wave functions and Coulomb interactions between electrons and holes for three types of InAs quantum dots: ~a! a free-standing spherical dot, ~b! a GaAs-embedded spherical dot, and ~c! a GaAs-embedded pyramidal dot. A comparison of ~a! and ~b! reveals the effects of strain, while a comparison of ~b! and ~c! reveals the effects of shape. We find that the larger band offsets in the ''free-standing'' dots ~i! produce greater quantum confinement of electrons and holes and ~ii! act to confine the wave functions more strongly within the dot, resulting in larger electron-hole Coulomb energies. The lower symmetry of the pyramidal dot produces a richer strain profile than the spherical dots, which splits the degeneracy of the hole states and polarizes the emitted light. @S0163-1829~99!02323-1#

I. INTRODUCTION

There are currently two leading methods for producing nanometer size semiconductor quantum dots. The first involves the controlled ripening of a lattice mismatched film, also called ''self-assembled,'' Stranski-Krastanow ~SK! growth.[1] In this approach the quantum dot material is deposited on top of a substrate with a different lattice constant, and

holes. Then the additional multiplicative factor @1 1 a_{4a}Tr(e)# is included to explicitly introduce strain dependence into the pseudopotential. We find that adjusting a_{4a} in this term allows the *absolute* LDA deformation potentials of the G_{15v}, G_{1c}, and X_{1c} states of bulk InAs and GaAs to be fitted. Without such a strain dependent term, only the *relative* deformations of $(G_{1c} \gtrsim G_{15v})$ and $(X_{1c} \gtrsim G_{15v})$ can be fit. Note, this trace term is not required in a self-consistent calculation. It is crucial in a non-self-consistent calculation to simulate the effects of the changes in the atomic positions on the potential.

In the InAs/GaAs heterostructures studied here, the strain dependence of the band offsets strongly effects the electron and hole confinement energies and it is therefore essential to accurately reproduce the *absolute* deformation potentials of the individual bands. In Eq. ~4!, Tr(e) is defined as $V(\mathbf{R})/V_0$, where $V(\mathbf{R})$ is the volume of the tetrahedron formed by the four nearest neighbors of the atom at $\mathbf{R}$ and V_0 is the volume of the same tetrahedron in the unstrained bulk. The fitted values of a_{0a}, a_{1a}, a_{2a}, a_{3a}, and a_{4a} are given for the InAs dot material and the GaAs barrier material in Table I. Note that the a_{4a} parameter is set to zero for As to avoid any ambiguity due to shared As atoms at InAs/GaAs interfaces.

For each system we construct a supercell containing the InAs dot with a chosen shape and a surrounding ''barrier material.'' For the embedded dots this barrier material is GaAs, while for the free-standing dot we passivate the surface dangling bonds by pseudoatoms representing a fictitious material with a very large band gap, designed to mimic the effects of vacuum. This artificial material is fitted to have the same lattice constant as InAs, so no strain is introduced into the system. In the GaAs-embedded InAs dot systems there is a 7% lattice mismatch between GaAs and InAs, so the atomic positions are first relaxed to their minimum strain energy values, using the valence force field ~VFF! elastic energy functional[12] before calculating the electronic structure. The VFF functional used in this

GaAs matrix is compressed in the direction perpendicular to the interface with the dot (e_{zz}), and expanded in directions parallel to the interface (e_{xx}, e_{yy}). The strain profiles in the GaAs matrix decay by approximately[18] $1/R^3$, where R is the distance from the center of the dot. The lower symmetry of the embedded pyramidal dot results in a much richer strain profile.[13] The tip of the pyramid expands in the horizontal directions (e_{xx}, e_{yy}), but is compressed in the vertical direction (e_{zz}). At the base of the pyramid, the InAs dot is constrained to adopt the GaAs substrate lattice constant, which results in compression in the horizontal directions (e_{xx}, e_{yy}), and a compensating expansion in the vertical direction (e_{zz}).

B. Strain-modified confining potentials

The effect of the above strain profiles on the electronic structure of the dots can be qualitatively understood by examining the strain-modified band offsets. These can be approximately calculated by coupling the electron and hole band edges to their deformation potentials. The electron band edge E_c couples only to the sum of the diagonal strain components,

$$E_c(e) = a_c(e_{xx} + e_{yy} + e_{zz}), \quad (7)$$

where a_c is the deformation potential of the conduction band at the Γ_{1c} point. The heavy- and light-hole band edges, E_{hh} and E_{lh}, couple to the individual strain components[19] according to

$$E_{hh}(e) = \frac{1}{3}(\Delta^{SO} + \Delta^{CF}),$$

$$E_{lh}(e) = -\frac{1}{6}(\Delta^{SO} + \Delta^{CF}) + \frac{1}{2}\sqrt{(\Delta^{SO} + \Delta^{CF})^2 - \frac{8}{3}}$$

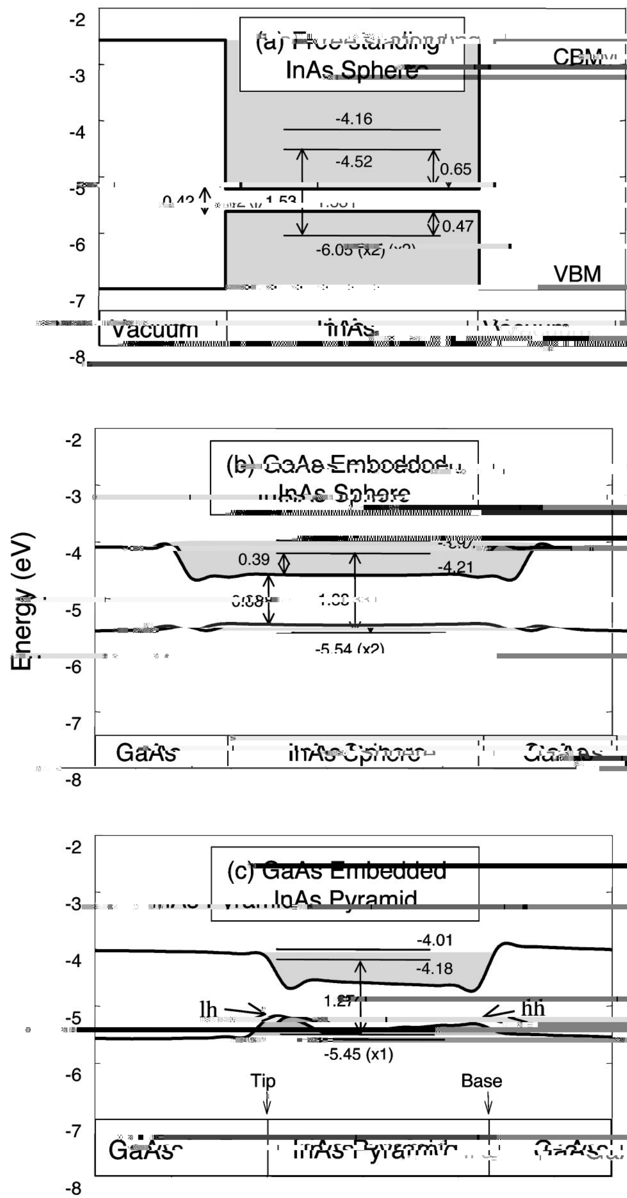

FIG. 3. Strain modified potential offsets for the CBM and VBM along a @001# line through the center of each dot. These are obtained by calculating the pseudopotential bulk band structures of InAs and GaAs in a supercell geometry, using the local strain of the dot ~Fig. 1!. The InAs/vacuum and InAs/GaAs offsets are shaded gray. The horizontal lines mark the energies of the confined electron and hole levels in the dots. These levels are calculated by using the folded spectrum method to find the band-edge eigenstates of the empirical pseudopotential Hamiltonian @Eq. ~1!#. All states are singly degenerate except where marked in brackets.

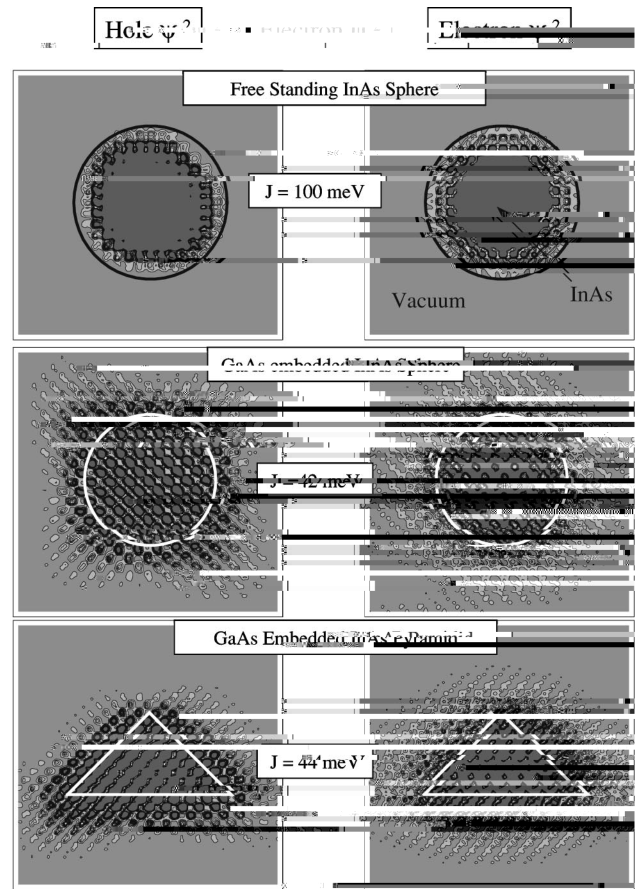

FIG. 4. Contour plots of the electron and hole wave functions in the $010% plane through the center of all three dots.

electron (E_c), heavy-hole, and light-hole (E_{hh}, E_{lh}) potential offsets in the $010% plane through the center of the dots. For both the spherical and pyramidal geometries, the InAs dots act as wells for both electrons and holes. In the spherical dot the confining wells are flat bottomed and adopt the spherical symmetry of the dot. In the lower symmetry, pyramidal case the wells are no longer flat-bottomed. The pyramidal electron well has two peaks, one near the tip and one near the base of the pyramid @see also below in Fig. 3~c!#. The pyramidal heavy- and light-hole wells have peaks at the base and tip, respectively @indicated by arrows in Fig. 2~b!#. The location of these peaks is implied by Fig. 1~b!, which shows that @$e_{zz} \gtrsim e_{xx}$#, and hence the crystal field splitting D^{CF} changes sign from positive at the base of the pyramid ($e_{zz}.\ e_{xx}$) to negative at the tip ($e_{zz},\ e_{xx}$). This change in sign results in the observed heavy-hole peak at the base of the pyramid ($D^{CF}.\ 0$) and light-hole peak at the tip of the pyramid ($D^{CF},\ 0$). Thus we expect that in the embedded spherical dot, electrons and holes will be attracted to the center of the dot, while in the pyramidal dot, electrons will also be attracted to the center of the dot but heavy holes will be attracted to the base of the pyramid and light holes attracted to the tip.

A more accurate picture of the strain-modified band edges can be obtained by calculating the energies of the bulk valence-band maximum ~VBM! and conduction-band maximum ~CBM! using our full pseudopotential subjected to the *local* strain produced by the dot. Figure 3 shows as thick lines the strain modified bulk band edges ~on an absolute scale with respect to vacuum! of the lowest energy conduction and highest energy valence states along a @001# line through the center of each of the three dot systems. These band edge energies are obtained by performing a series of *bulk* calculations using the local strain in the dot, $e(\mathbf{R})$, at a series of points along the line $\mathbf{R}$. Within the small strain regime where deformation potential theory is applicable, the energy of the CBM's in Fig. 3 correspond to the electron band edges in Fig. 2, while the energy of the highest hole

corresponds to the heavy hole for the spherical dots and a combination of the heavy hole near the base and light hole near the tip for the pyramidal dot.

The two lowest confined electron and highest hole energy levels of the Hamiltonian in Eq. ~1! are plotted as thin horizontal lines. These were calculated using the folded spectrum method @Eq.~5!# where the reference energy e_{ref} was placed

tronic structure of the dots is strongly affected by the size of the band offsets, but not so strongly affected by their geometry.

IV. SUMMARY

We have performed fully atomistic, pseudopotential calculations of free-standing and GaAs-embedded, spherical and pyramidal InAs quantum dots. The valence- and conduction-band offsets between the free-standing InAs dot and vacuum are much larger than between GaAs and the embedded InAs dots. The larger offsets in the free-standing system produce greater quantum confinement of the energy levels and therefore a larger confined electron to a confined hole band gap. They also increase the localization of the electron and hole wave functions within the dot, which in turn increases the electron-hole Coulomb energy and decreases the electron-hole dipole transition matrix element. The lower symmetry of the pyramidal dot, produces a richer strain profile than the spherical dots, that splits the degeneracy of the VBM states, reduces the quantum confinement of the wave functions still further and polarizes the emitted light.

ACKNOWLEDGMENTS

This work was supported by the DOE, Basic Energy Sciences, Division of Materials Science under Contract No. DE-AC36-83CH10093. The authors thank L.W. Wang and S.H. Wei for useful discussions.

[1] N. Carlsson *et al.*, J. Cryst. Growth **170**, 1271 ~1997!.
[2] K. Schmidt, G. Medeiros-Ribeiro, M. Oestreich, and P. Petroff, Phys. Rev. B **54**, 11 346 ~1996!.
[3] G. Solomon, J. Trezza, A. Marshall, and J. Harris, Phys. Rev. Lett. **76**, 952 ~1996!.
[4] N. Carlsson, W. Seifert, A. Petersson, P. Castrillo, M. E. Pistol, and L. Samuelson, Appl. Phys. Lett. **66**, 3093 ~1994!.
[5] A. Henglein, Chem. Rev. **89**, 1861 ~1998!.
[6] L. Brus, J. Phys. Chem. Solids **59**, 459 ~1998!.
[7] D. Norris and M. Bawendi, Phys. Rev. B **53**, 16 338 ~1996!.
[8] M. Chamarro, V. Voliotis, R. Grousson, P. Lavallard, T. Gacoin, G. Counio, J. P. Boilot, and R. Cases, J. Cryst. Growth **159**, 853 ~1995!.
[9] D. Bertram, O. Micic, and A. Nozik, Phys. Rev. B **57**, R4265 ~1998!.
[10] U. Banin, J. C. Lee, A. A. Guzelian, V. Kadavanich, A. P. Alivisatos, W. Jaskolski, G. W. Bruant, Al. L. Efros, and M. Rosen, J. Chem. Phys. **109**, 2306 ~1998!.
[11] L.-W. Wang and A. Zunger, Phys. Rev. B **51**, 17 398 ~1995!.
[12] P. Keating, Phys. Rev. **145**, 637 ~1966!.
[13] C. Pryor, J. Kim, L.-W. Wang, A. Williamson, and A. Zunger, J. Appl. Phys. **83**, 2548 ~1998!.
[14] R. Martin, Phys. Rev. B **1**, 4005 ~1970!.
[15] A. Silverman, A. Zunger, R. Kalish, and J. Adler, J. Chem. Phys. **100**, 2394 ~1994!.
[16] L.-W. Wang and A. Zunger, J. Chem. Phys. **100**, 2394 ~1994!.
[17] L.-W. Wang and A. Zunger, *Semiconductor Nanoclusters* ~Elsevier Science, Amsterdam, 1996!.
[18] J. Eshelby, J. Appl. Phys. **25**, 255 ~1954!.
[19] S.-H. Wei and A. Zunger, Phys. Rev. B **49**, 14 337 ~1994!.
[20] A. Williamson and A. Zunger, Phys. Rev. B **58**, 6724 ~1998!.
[21] H. Haken, Nuovo Cimento **10**, 1230 ~1956!.